PROCEEDINGS OF SCIENCE

Direct determination of the ^{11}C$(\alpha,p)^{14}$N reaction rate with CRIB: an alternative synthesis path to the CNO elements

S. Hayakawa*, **S. Kubono, T. Hashimoto, H. Yamaguchi, D.N. Binh, D. Kahl**
Center for Nuclear Study, Graduate School of Science, University of Tokyo
E-mail: hayakawa@cns.s.u-tokyo.ac.jp

Y. Wakabayashi

Advanced Science Research Center, Japan Atomic Energy Agency

N. Iwasa, N. Kume, Y. Miura

Department of Physics, Tohoku University

T. Teranishi

Department of Physics, Kyushu University

J.J. He

Institute of Modern Physics, Chinese Academy of Science

Y.K. Kwon

Department of Physics, Chung Ang University

T. Komatsubara

Department of Physics, University of Tsukuba

S. Kato

Department of Physics, Yamagata University

S. Wanajo

Max-Plank Institut fúr Astrophysik

We reported new results on the first direct measurement of the ^{11}C$(\alpha,p)^{14}$N reaction, which is considered to be part of an alternative pathway responsible for the nucleosynthesis from the pp-chain region to the CNO cycle region in high-temperature hydrogen burning processes. We successfully measured the excitation functions at stellar energies both for (α,p_0), (α,p_1) and (α,p_2) separately for the first time.

11th Symposium on Nuclei in the Cosmos
19-23 July 2010
Heidelberg, Germany.

*Speaker.

PoS(NIC XI)062

1. Introduction

The $^{11}\mathrm{C}(\alpha,p)^{14}\mathrm{N}$ reaction is considered to be part of a pathway responsible for the nucleosynthesis from the pp-chain region to the CNO region, in addition to the well-known triple-alpha process. This reaction path is likely to be effective in extremely high-temperature hydrogen burning processes, such as the breakout process from the hot pp-chains [1] in low-metallicity stars, or the νp-process in core-collapse supernovae. Recent simulations of the νp-process [2] suggest that the $^{7}\mathrm{Be}(\alpha,\gamma)^{11}\mathrm{C}$ reaction, mostly flowing to the subsequent reaction $^{11}\mathrm{C}(\alpha,p)^{14}\mathrm{N}$, considerably contributes and eventually affects the abundance pattern of the p-nuclei around $A = 90$–110. It is important to know the $^{11}\mathrm{C}(\alpha,p)^{14}\mathrm{N}$ reaction rate to review its contribution in the pathway. There are reaction rate data sets of this reaction available from the time-reversal reaction measurements with the activation method [3] or the Hauser-Feshbach statistical model calculations by the code NON-SMOKER$^{\mathrm{WEB}}$ [4]. However, the former provides only the $^{11}\mathrm{C}(\alpha,p_0)^{14}\mathrm{N}$ reaction rate, and the latter has no information on resonances, and thus none of them could provide a correct reaction rate. In order to resolve this issue, we have performed the first-ever direct measurement of the $^{11}\mathrm{C}(\alpha,p)^{14}\mathrm{N}$ reaction cross sections aiming at measuring separately the proton decays to the different states in $^{14}\mathrm{N}$ in the $^{11}\mathrm{C}(\alpha,p)^{14}\mathrm{N}$ reaction in the center-of-mass energy range from 1 to 4.5 MeV, including the Gamow windows from 1.5 to 3 GK of astrophysical interest.

2. Experiment

The measurements were performed by means of the thick-target method [5] in inverse kinematics with secondary beams produced by CRIB (CNS Radioactive Ion Beam separator) at the Center for Nuclear Study (CNS), the University of Tokyo [6]. We used two $^{11}\mathrm{C}$ beams at different kinetic energies to cover a wide excitation energy range in $^{15}\mathrm{O}$, and a $^{11}\mathrm{B}$ beam for calibration with the known $^{11}\mathrm{B}(\alpha,p)^{14}\mathrm{C}$ reaction cross sections [7, 8]. The $^{11}\mathrm{B}^{3+}$ primary beam was provided by the RIKEN AVF cyclotron at 4.6 MeV/u with a maximum intensity of 1 pμA. The secondary beam particles $^{11}\mathrm{C}$ were produced via the $^{1}\mathrm{H}(^{11}\mathrm{B},^{11}\mathrm{C})n$ reaction with a 1.2–1.7-mg/cm^2-thick cryogenic hydrogen gas target. The energy of the $^{11}\mathrm{B}$ beam for the calibration run was degraded with the same target condition as above. The energy losses of the secondary beams in the secondary $^{4}\mathrm{He}$ gas target were directly measured separately from the reaction measurement runs with a Si detector at 5 different gas thicknesses from 0 to 1.24 mg/cm^2. The beam conditions used for the experiment are summarized in Table 1.

A schematic plane view of the experimental setup is illustrated in Fig. 1. We used two types of beam monitors (*i.e.* Parallel Plate Avalanche Counters (PPAC1, PPAC2) and/or a Microchannel Plate (MCP) detector) for beam trajectory and timing measurement. The different incident $^{11}\mathrm{C}$ energies were produced by switching between PPAC2 and the MCP mounted as the second beam

Table 1: Secondary beam conditions used for the experiment

Beam particle	E_{cm} range [MeV]	Beam rate [pps]	Purity [%]	2nd beam monitor
$^{11}\mathrm{C}^{6+}$	2.3–4.5	1.0×10^{5}	$\sim$100	MCP
$^{11}\mathrm{C}^{6+}$	0.0–2.7	3.1×10^{5}	$\sim$100	PPAC2
$^{11}\mathrm{B}^{5+}$	2.9–4.5	2.6×10^{5}	$\sim$100	PPAC2

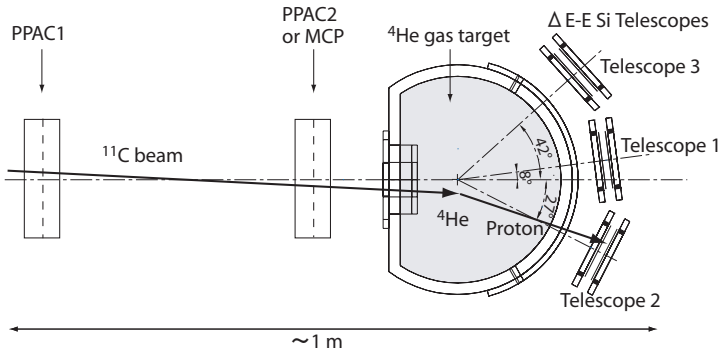

Figure 1: Schematic plane view of the experimental setup

monitor. The target had a semi-cylindrical shape whose length from the entrance to the exit on the beam axis was 140 mm. ^{4}He gas of 400 Torr was confined by a 2.5-μm-thick Havar foil at the entrance and a 25-μm-thick Mylar foil at the exit. The incident ^{11}C beam energy of 10.1 MeV and 16.9 MeV covered the center-of-mass energy range of 0–4.5 MeV in the ^{4}He gas target. Recoil protons and α particles, as well as small numbers of deuterons and ^{3}He particles, were clearly identified with ΔE-E silicon telescopes. Each ΔE counter was a double-sided stripped silicon detector and the E counter was a single-pad silicon detector.

3. Analysis and Results

We successfully identified the final states in ^{14}N from the time-of-flight information of the reaction particles between PPAC1 and the SSDs and the kinetic energy of the recoil protons, as each transition for a given recoil proton energy takes place at a different position in the target. The proton events with the high- and low-energy beams are shown in Fig. 2-(a) and (b) respectively, where the ordinates indicate the time difference with respect to the (α,p_0) time while the abscissae indicate the kinetic energies of protons. The time difference and energy range of the (α,p_1) and (α,p_2) are consistent with the calculation, so that we can identify them as illustrated in Fig. 2. In the low-energy run, the (α,p_0) and (α,p_1) can be separated relatively easily, and only a narrow energy range of the (α,p_2) is energetically allowed in addition. In the high-energy run, the (α,p_1) events could partially overlap the (α,p_0) and (α,p_2), but its effect should be sufficiently small as its yield apparently much lower in the overlapping region. For a (α,p_2) excitation function, the higher energy part down to the onset of the (α,p_3) is used. Currently, only clearly-identified regions marked with hatched lines in Fig. 2 are used for the excitation functions in Fig. 3.

The center-of-mass energy, as well as the scattering angle, can be uniquely reconstructed with the kinematic quantities, such as the beam energy loss distribution in the target, the beam track, the proton energy, and the proton detection position. The detection efficiency at each center-of-mass angle and energy are calculated based on the Monte Carlo simulation. At present, the cross section was determined assuming isotropy, with the error bars indicating the statistical error and the deviation from isotropy. In Fig. 3, the newly determined excitation functions for the (α,p_0), (α,p_1) and (α,p_2) are plotted. The (α,p_0) function of this work is mostly found to be consistent with the excitation function deduced from the time-reversal reaction data [9] via the principle of

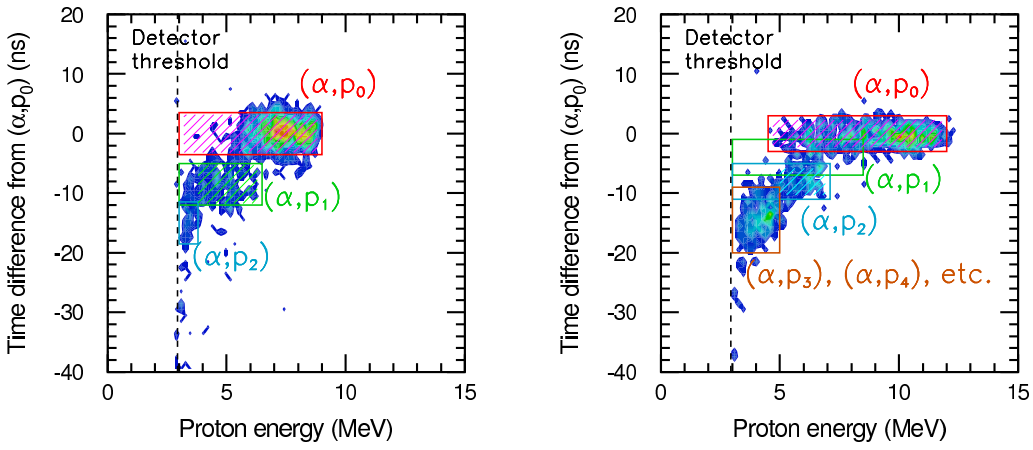

(a) Low-energy run (b) High-energy run

Figure 2: Identification of the protons at the 27° telescope. Each abscissa indicates the proton energy and each ordinate indicates the time difference with respect to the (α, p_0) events with (a) the low-energy beam and (b) the high-energy beam. The data in hatched areas correspond to the excitation functions in Fig. 3.

detailed balance, except around some resonances at lower energies. The (α, p_0) functions for the low- and the high-energy run show a good consistency in their overlapping region. The (α, p_1) covers the stellar temperatures up to 3 GK where the (α, p_2) cross section can be extrapolated to be sufficiently small.

Figure 4 shows a summary of the relative reaction rates obtained by the present work, the NON-SMOKER$^{\mathrm{WEB}}$ [4], and the time-reversal reaction labeled "CF88" [3], which is the one currently accepted. The newly obtained reaction rate for the $(\alpha, p_{0,1,2})$ differs from either CF88 or

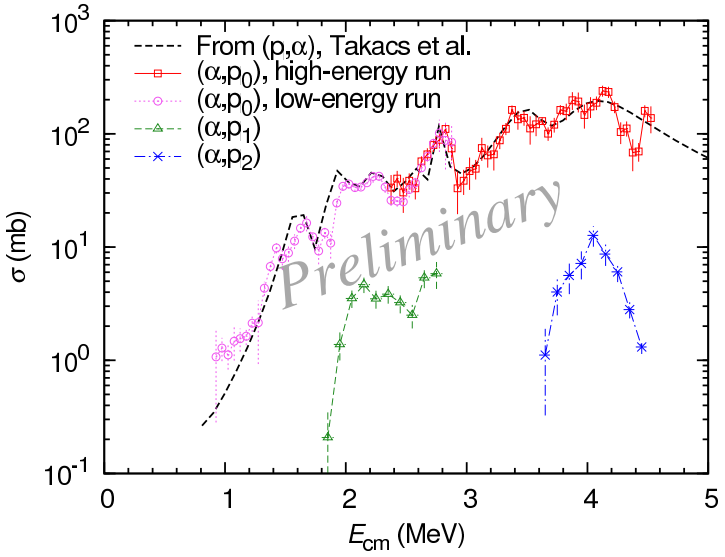

Figure 3: Excitation functions of the $^{11}\mathrm{C}(\alpha, p_0)^{14}\mathrm{N}$ (Low-energy run: magenta circle, high-energy: red square), $^{11}\mathrm{C}(\alpha, p_1)^{14}\mathrm{N}^*$ (green triangle), and $^{11}\mathrm{C}(\alpha, p_2)^{14}\mathrm{N}^*$ (blue cross) reactions. The black dashed line is obtained from the previous time-reversal reaction studies [9].

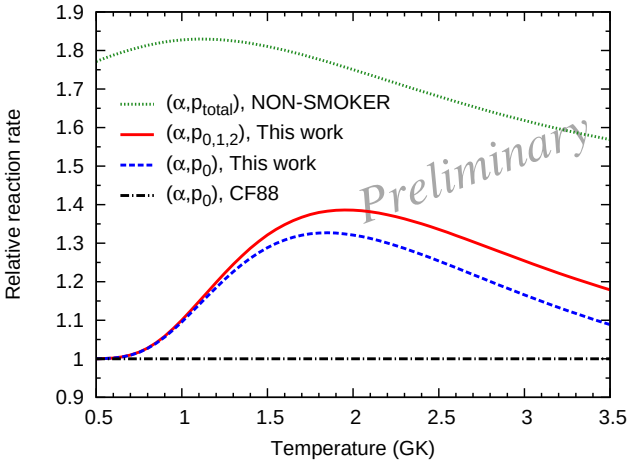

Figure 4: Comparison of the relative reaction rates among the NON-SMOKER$^{\mathrm{WEB}}$ calculation [4] (dotted line), the $(\alpha, p_{0,1,2})$ reaction of this work (solid line), and the (α, p_0) reaction of this work (dashed line) to the time-reversal reaction data (dashed-dotted line).

NON-SMOKER$^{\mathrm{WEB}}$. A more detailed discussion requires further works; the angular distributions of the differential cross sections are being analyzed for more proper integrations instead of assuming isotropy.

4. Conclusions

We successfully observed the (α, p_0), (α, p_1) and (α, p_2) transitions separately and determined their preliminary excitation functions. The resonant shapes and absolute values of the (α, p_0) excitation function agree reasonably well with the ones from the time-reversal reaction data over the energy range of measurement. Although the (α, p_1), (α, p_2) excitation functions can be deduced only in the limited energy ranges, they are still useful to estimate their contribution to the total reaction rates at the stellar temperatures of 1.5–3 GK. But the conclusive reaction rate requires a more reliable total excitation function with a careful treatment of the angular distribution.

References

[1] M. Wiescher *et al.*, Astrophys. J. **343** (1989) 352.

[2] S. Wanajo *et al.*, arXiv:1004.4487v1 (2010).

[3] G. Caughlan and W. Fowler, Atomic data and nuclear data tables **40** (1988) 283.

[4] T. Rauscher, http://nucastro.org/reaclib.html#ns_web .

[5] K.P. Artemov *et al.*, Sov. J. Nucl. Phys. **52** (1990) 480.

[6] Y. Yanagisawa *et al.*, NIM A **539** (2005) 74.

[7] n R. Bonetti, A. Guglielmetti and G. Poli, Appl. Radiat. lsot. **48** (1997) 873.

[8] L.L. Lee, Jr., J.P. Schiffer, Phys. Rev. **115** (1959) 160.

[9] Takács *et al.*, NIM B **240** (2005) 790.